European Journal of Oral Sciences

Eur J Oral Sci 2019; 127: 276–284
DOI: 10.1111/eos.12617

European Journal of Oral Sciences

Effect of interface surface design on the fracture behavior of bilayered composites

Tarek A. Omran[1,2,3], Sufyan Garoushi[2,3], Lippo V. Lassila[2,3], Pekka K. Vallittu[2,3,4]

[1]Finnish Doctoral Program in Oral Sciences (FINDOS), Turku; [2]Department of Biomaterials Science, Institute of Dentistry, Faculty of Medicine, University of Turku, Turku; [3]Turku Clinical Biomaterials Centre (TCBC), Turku; [4]City of Turku Welfare Division, Oral Health Care, Turku, Finland

Omran TA, Garoushi S, Lassila LV, Vallittu PK. Effect of interface surface design on the fracture behavior of bilayered composites.
Eur J Oral Sci 2019; 127: 276–284. © 2019 Eur J Oral Sci

This study aimed to evaluate the effect of different interface designs on the load-bearing capacity of bilayered composite structures (BLS). Cylindrical specimens of BLS were prepared from base composite of 3.5 mm thickness and surface composite of 1.5 mm thickness ($n = 80$). Two different base composites – flowable bulk-fill (FBF) [smart dentin replacement (SDR)] and short fiber-reinforced (FRC) (everX Posterior) – were evaluated, and conventional composite (G-ænial Posterior) was used as the surface layer. Four different interface designs were used: (i) pyramidal; (ii) mesh; (iii) linear grooves; and (iv) flat surface (control). Three-dimensional printed molds were fabricated to standardize the interface design between the surface and the base composites. The specimens were then statically loaded with a steel ball until fracture using a universal testing machine. Fracture types were classified into catastrophic, complete, and partial bulk. ANOVA revealed that both the material and the interface design had a statistically significant effect on the load-bearing capacity. Flowable bulk-fill showed lower mean load-bearing capacity than FRC in all the interface designs tested, except for the flat surface design. Fracture analysis showed that FRC demonstrated up to 100% partial bulk fractures with the pyramid interface design, but no incidence of catastrophic bulk fracture. By contrast, FBF demonstrated up to 84.6% and 40% catastrophic bulk fractures with the flat interface design but no incidence of partial bulk fracture. Consequently, the interface designs studied enhanced the fracture behavior of BLS.

Tarek A. Omran, Department of Biomaterials Science, Institute of Dentistry, University of Turku, Lemminkäisenkatu 2, FI-20520 Turku, Finland

E-mail: tarek.omran@utu.fi

Key words: bulk-fill composite; biomimetic restoration; dentin–enamel junction; fiber reinforced composite; 3D modeling

Accepted for publication March 2019

Direct restorative procedures are routine interventions in clinical dentistry, and posterior composite restorations, in particular, present the most challenging of these interventions (1–3). Minute discrepancies in filling techniques may lead to premature failure of the restoration, making composite filling materials technique-sensitive (4, 5). Hence, a closer look at the filling techniques used for restorative treatment is important in view of the potential magnitude of their repercussions (6).

Since the popularization of the SiSta classification system by Mount *et al.* (7) regarding cavity design, minimally invasive dentistry has become the optimal standard of care (8). Improvements in both composite filling materials and bonding procedures allow for minimally sized cavities, without the need for unnecessary loss of healthy tooth structure in order to achieve mechanical retention (9). Therefore, the primary reference for cavity design is removal of the active carious lesion. Cavity design is thus not predetermined by the mechanical properties of the composite materials but rather by preserving the greatest amount of healthy tooth structure (10). However, the actual difference in material properties between different composite materials remains a factor that needs to be taken into account (11).

In recent years, novel materials, such as bulk-fill and discontinuous short-fiber reinforced composites, have gained traction in the clinical setting, and numerous studies have shown the promising performance of these materials (11, 12). Bulk-fill materials are indicated to be placed and light cured in bulk increments, of up to 4 mm, in medium-to-large posterior cavities (13, 14). Such materials have the benefit of an increased depth of cure as a result of the amount of filler, their translucency, and the presence of additional photo-initiators (15). These factors lead to shorter application times in comparison with the increments of 2 mm used for conventional particulate filler composite (16).

Moreover, the conventional incremental technique poses the risk of incorporation of voids and the introduction of an unreacted composite monomer layer, known as the oxygen inhibition layer, between the many successive layers (17). It is known that both aforementioned factors affect the performance of the

restorations and thus reducing their incidence would be beneficial (18, 19).

Bulk-fill materials also exist with varying material properties, being packable and flowable (20). In comparison to conventional particulate filler composites flowable bulk-fill composites have less filler content and hence are able to flow to fill the deeper areas of posterior cavities, and their less-viscous material properties have been reported to improve their clinical performance as a result of the decreased polymerization stress and cuspal strain (20–22). However, the decreased filler content also results in decreased wear resistance and therefore flowable bulk-fill composites need to be covered occlusally using a conventional particulate filler composite (13). A well-known material from this category uses the brand name Smart Dentin Replacement (SDR), which is intended to be used as a dentin replacement in posterior restorations (23).

By contrast, fiber-reinforced composites have short discontinuous glass fibers as a filler, which has been reported to improve the mechanical properties (such as increasing fracture resistance and deflecting crack propagation) of large restorations (24, 25). One material from this category uses the brand name everX Posterior and, similarly to flowable bulk-fill composite, can also be placed in bulk (26). Fiber-reinforced composites have been shown to possess high fracture toughness (27). Nonetheless, they must also be coated with a top layer of conventional particulate filler composite to protect the fibers and improve the wear resistance during masticatory function (28).

As a result, such bulk-fill and short fiber-reinforced materials give rise to a bilayered composite structure that integrates two different composite materials exhibiting two differing properties: a top layer with high wear resistance to the masticatory function; and a bottom layer that forms the supporting bulk (29). In principle, such a bilayered configuration is similar to that of a natural tooth (i.e., a top layer of wear-resistant enamel and a bottom layer of supporting dentin bulk) (30, 31).

Furthermore, the natural configuration of the interface between dentin and enamel is an intricate design of dentin–enamel junction scallops, which form a gradient-like interface (32). The dentin–enamel junction is known to have a protective function toward fracture propagation by either deflecting or hindering crack formation (30, 31, 33).

It has been reported that using a bilayered biomimetic approach as a filling technique can improve mechanical behavior through utilizing the inherent strengths of each material, while reducing the total number of layers needed to restore the cavity (34–36).

However, as far as the authors are aware, a detailed guideline, such as the minimally invasive cavity design presented by Mount *et al.* (7), does not yet exist for bilayered restorations. If a bilayered filling technique is to be optimized, factors such as the properties of the materials used, the thickness of each layer, the quality of adhesion of the composite–composite interface, and the interface design between the two layers would be beneficial areas of study.

In this work, we study the interface design between the different composite materials. Typically, dentists apply bulk-fill composites so that their surface is flat, before applying the final top layer of particulate filler composite. Inevitably, an oxygen-inhibited layer of unreacted monomer forms on the surface of a freshly light-cured base composite, causing a distinct margin between the two layers (17).

The aim of this study was therefore to fabricate interface designs that could be imprinted on the surface of different bulk-fill composites before applying the final top layer of particulate filler composite. Such a design can offer a gradient-like interface similar to that of the dentin–enamel junction. In addition, these bilayered structures were mechanically loaded to investigate the effect of the interface designs on fracture behavior. The following null hypotheses were tested: (i) fracture behavior would not be affected by the different interface designs; and (ii) there would be no significant differences in fracture behavior using different bulk-fill composite materials.

Material and methods

Interface design fabrication

In this study, four interfacial designs were prepared using the three-dimensional (3D) modeling computer software, Rhinoceros 5 (Mc Neel Europe, Barcelona, Spain) (Fig. 1). The finalized interfacial designs were then 3D printed using a Form2 3D printer (FormLabs, Somerville, MA, USA). The printer utilized stereolithography technology and methacrylate photopolymer resin.

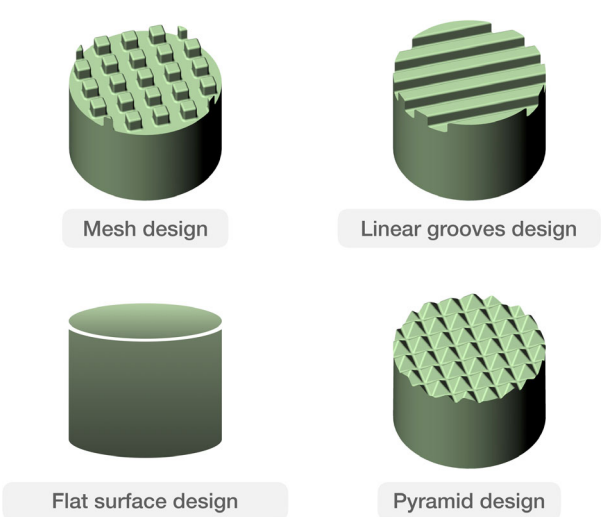

Fig. 1. Computer-rendered three-dimensional (3D) models of the interface designs used in this study. The width and depth of the grooves in the mesh and linear designs are 0.5 mm. In the pyramid design, the width of the groove is 1 mm and the depth is 0.5 mm.

Subsequently, transparent polyvinyl siloxane elastomer molds (Memosil 2; Kulzer, Mitsui Chemicals, Tokyo, Japan) were fabricated so that they could be pressed onto the base composite to produce the following four designs: pyramidal; mesh; linear grooves; and flat surface (Fig. 1).

The four interface designs produced on the surface of the base composites were profiled with a 3D optical microscope (Bruker Nano, Berlin, Germany) using VISION64 software (Tucson, AZ, USA). The maximum interface design depth values (μm), representing the average of the lowest or deepest points of all profile scans, were calculated from different points.

Specimen preparation

Eighty bilayered cylindrical specimens were prepared using transparent cylindrical plastic molds (diameter: 7 mm; total height: 5 mm). Four interface-design test groups were fabricated using each of the base composites ($n = 10$ per group).

All bilayered specimens comprised a bottom layer made of a base composite of either everX Posterior (GC, Tokyo, Japan), which is a short fiber-reinforced bulk-fill base composite, or SDR (Dentsply Sirona, York, PA, USA), which is a flowable bulk-fill composite. A top layer of G-ænial Posterior (GC, Tokyo, Japan), which is a conventional particulate filler composite (Table 1), was added. The exact thickness of each layer is presented in Fig. 2.

After placing the base composite materials in the cylindrical plastic molds, a transparent polyvinyl siloxane elastomer mold with the appropriate interface design was pressed onto the surface of the base composites to imprint the interface design onto the surface of the base composite before light curing. A light-emitting diode (LED) light-curing unit (Elipar S10; 3M ESPE, St Paul, MN, USA) was calibrated using MARC Resin Calibrator (BlueLight Analytics, Halifax, Canada). A calibrated average light intensity of 1,765.30 mW cm^{-2} (SD = 17.91) was used throughout this study.

The specimens were initially light cured from the top surface and through the transparent polyvinyl siloxane elastomer mold for 5 s. Then, the molds were immediately removed and the light curing process was continued for 35 s. Finally, a top layer of particulate filler composite was used to cover the base composite and was light cured for 40 s from the top surface.

The prepared specimens were stored for 48 h in a dry environment at room temperature (23 ± 1°C) before they were tested.

Compression test and fracture analysis

The specimens were subject to static loading with a steel ball (Ø 4 mm), placed perpendicular to the top layer of the specimens until fracture, using a universal testing machine (Model LRX; Lloyd Instruments, Fareham, UK). The contact point of the steel ball on the specimen was at the middle of the specimen, and the extension rate was 1 mm min^{-1}. Testing was carried out at room temperature (23 ± 1°C), and loading data were computed using PC software (Nexygen; Lloyd Instruments).

Fracture patterns were then visually examined by three different examiners and placed into four categories:(i) Catastrophic was the most unfavorable type of fracture pattern as the entire bilayered specimen completely shattered into several pieces(ii) Complete bulk fracture was declared when the fracture went through the bulk material and split the specimen in half, rendering a poor outcome for repair (iii) Partial bulk fracture presented a more favorable fracture pattern. This is because the fracture lines ran more superficially and away from the midline of the specimen, which preserved most of the bulk of the remaining material (Fig. 2)(iv) Adhesive fracture was identified when the fracture line advanced along the interface without involvement of the base composite in the bilayered structures.

Surface microhardness test

It is known that atmospheric oxygen forms a layer of unreacted monomer on the surface of freshly light-cured composite materials (18). Therefore, surface microhardness [Vickers hardness number (VHN)] measurements were carried out to analyze the interface design fabrication technique and light-curing protocol used in this study and its effect on the surface of the base composites fabricated. It has been reported that surface microhardness has a correlation with the degree of monomer conversion (DC%) (37, 38). Therefore, this could affect the physical properties of the specimen.

The surface microhardness measurements (five points for each specimen) were carried out using a universal Vickers device (Struers Duramin, Struers, Ballerup, Denmark), with a load of 245.3 mN being applied for 15 s.

Table 1

Materials used in this study

Material (Shade)	Code name	Lot No.	Manufacturer	Type of composite	Matrix composition	Inorganic filler content
G-ænial Posterior (A3)	GP	1501071	GC, Tokyo, Japan	Micro-hybrid conventional	UDMA, dimethacrylate comonomers (Bis-GMA free)	Prepolymerized fillers with silica filler content 81 wt% 65 vol%
EverX Posterior (n/a)	FRC	1601081	GC, Tokyo, Japan	Discontinuous fiber reinforced	Bis-GMA, PMMA, TEGDMA	Short E-glass fiber filler, barium glass 74.2 wt%, 53.6 vol%
SDR (universal)	FBF	1611111	Dentsply Sirona, York, PA, USA	Flowable bulk-fill	TEGDMA, EBADMA	68 wt%, 44 vol%, barium borosilicate glass

Bis-GMA, bisphenol-A-glycidyl dimethacrylate; EBADMA, ethoxylated bisphenol-A-dimethacrylate; PMMA, polymethylmethacrylate; TEGDMA, triethylene glycol dimethacrylate; UDMA, urethane dimethacrylate; vol%, volume percentage; wt%, weight percentage.

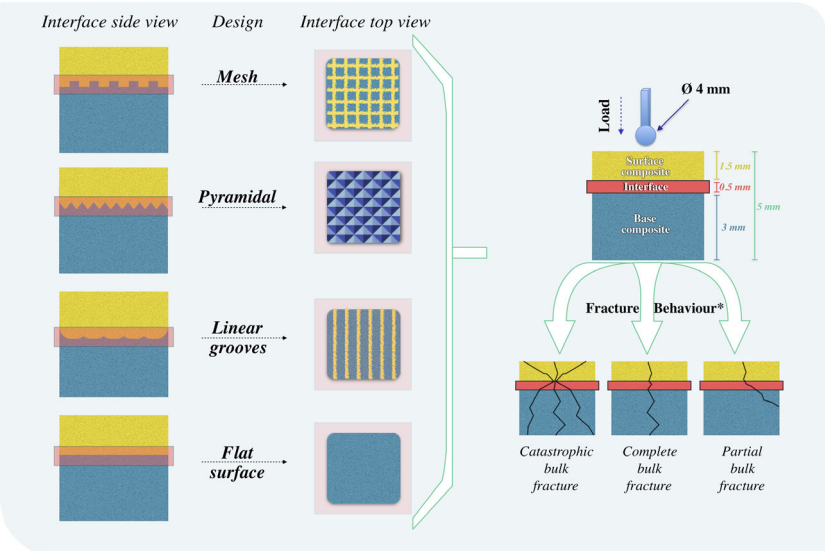

Fig. 2. Two-dimensional schematic illustrations of the specimens and the different interface designs investigated in this study. Loading set up is demonstrated on the right. Fracture behavior was categorized into catastrophic fracture, complete bulk fracture, or partial bulk fracture.

The time elapse between the point of indentation and the measurement of the deformation produced was standardized at 30 s to equate for possible elastic recovery of deformation after the point of indentation (39, 40). Test indentations should be performed on a flat surface and therefore the flat interface design was chosen for surface microhardness testing.

The length of the diagonal of each indentation was measured directly using a graduated eye-lens. The VHN was obtained using the following equation:

$$H = \frac{1{,}854.4 \times P}{d^2}$$

where H is Vickers hardness (kg mm^{-2}), P is the load (g), and d is the length of the diagonals (μm).

Furthermore, three test protocols were prepared to test the surface microhardness of each of the base composite materials (n = 4 per group) (3.5-mm-thick cylinders with a diameter of 7 mm).

Test protocol 1: current study light-cure protocol: The flat polyvinyl siloxane elastomer mold was placed touching the base composite, and was light-cured for 5 s. Then, the polyvinyl siloxane elastomer mold was immediately removed and light curing was continued for 35 s. Specimens were tested immediately after light polymerization.

Test protocol 2: conventional light-cure protocol used in clinics; exposure to atmospheric oxygen: The base composite was light cured directly for 40 s without using the polyvinyl siloxane elastomer mold. Specimens were tested immediately after light polymerization.

Test protocol 3: protected from atmospheric oxygen: A microscope glass slab was placed on the base composite surface, after which the specimens were light polymerized. The glass slab was kept in contact with the base composite for an additional 360 min. Afterwards, the glass slab was removed, and the surface microhardness of the specimens was measured.

Statistical analysis

Maximum load values in the compression test were analyzed using two-way ANOVA followed by Tukey's post-hoc analysis, at a significance level of $P < 0.05$, using SPSS software (SPSS, Chicago, IL, USA).

Results

Compression test and fracture analysis

Two-way ANOVA revealed that the material and the interface design had a significant effect on the load-bearing capacity ($P < 0.05$). The mean load values acquired at maximum compression are presented in Fig. 3. The mean load values for the flat interface designs were higher than those for other interface designs, for both base materials. For the flowable bulk-fill composite (SDR), a change in interface design significantly affected the loads acquired ($P < 0.05$). For fiber-reinforced composite (everX), only the mesh interface design showed statistically different load values from the other interface designs investigated ($P < 0.05$).

Fracture types are summarized in Table 2 and shown in Fig. 4. No adhesive or partial bulk fractures were identified for flowable bulk-fill composite (SDR) groups. The two modes of fracture observed for flowable bulk-fill composite were catastrophic fracture and complete bulk fracture, and the interface design was found to influence the percentage of these fracture modes. The descending order of percentage of catastrophic fractures with relation to interface design was as follows: Flat

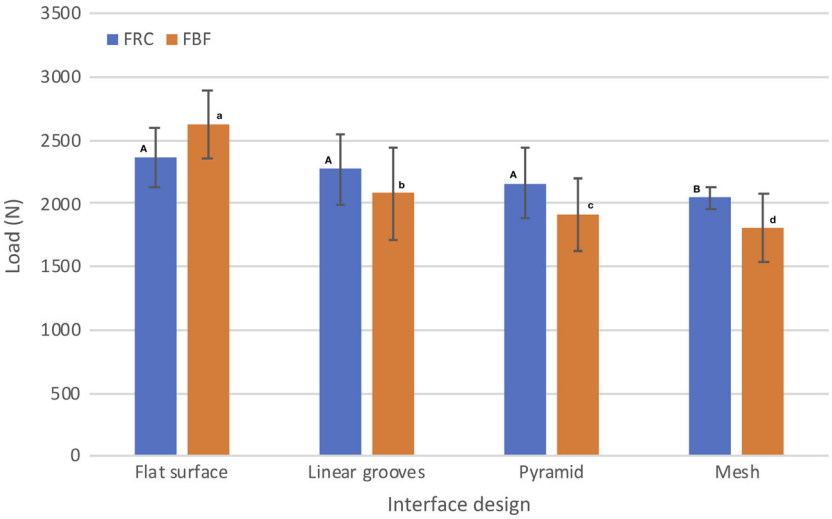

Fig. 3. Investigation of load-bearing capacities ($N \pm SD$), for the interface designs tested in this study, which were sited between the surface particulate filler composite and the base composite. The same superscript upper-case letter represents a non-statistically significant difference ($P > 0.05$, Tukey's post-hoc testing) between material and interface design in fiber-reinforced composite (FRC) groups (everX). The same superscript lower-case letter in a column represents a non-statistically significant difference ($P > 0.05$, Tukey's post-hoc testing) between material and interface design in flowable bulk fill composite (FBF) groups (SDR).

Table 2

Results of fracture pattern assessment for all bilayered groups

Interface design	Base material	Percentage of different types of failure			
		Catastrophic bulk fracture	Complete bulk fracture	Partial bulk fracture	Adhesive fracture
Flat surface	FBF	84.6	15.4	–	–
	FRC	–	36.4	63.6	–
Linear grooves	FBF	54.5	45.5	–	–
	FRC	–	30.0	70.0	–
Mesh	FBF	50.0	50.0	–	–
	FRC	–	20.0	80.0	–
Pyramid	FBF	40.0	60.0	–	–
	FRC	–	0.0	100.0	–

FBC, flowable bulk-fill composite (SDR); FRC, fiber-reinforced composite (everX).

surface > Linear grooves > Mesh > Pyramid (84.6%, 54.4%, 50%, and 40%, respectively).

No adhesive or catastrophic fractures were identified for fiber-reinforced composite (everX). The two modes of fracture observed for fiber-reinforced composite were partial fracture and complete bulk fracture, and the interface design was found to influence the percentage of these fractures. The ascending order of percentage of partial bulk fractures in relation to interface design was as follows: Flat surface > Lines > Mesh > Pyramid (63.6%, 70%, 80%, and 100%, respectively).

Surface microhardness test

Test Protocol 3 was the only protocol that yielded measurable indentations. Fiber-reinforced composite (everX) (VHN: 61.8 ± 2.5) showed higher hardness values than flowable bulk-fill composite (SDR) (VHN: 30.9 ± 1.7).

Discussion

In the present study, the concept of fabricating an interface design was inspired by the dentin–enamel junction, which is known to be scalloped in nature (41). Several studies have looked closely at this natural interface and closely investigated its structure and behavior (30, 31, 42, 43).

However, there is no biomimetic model for bilayered restorations. According to Brauer *et al.* (32), who investigated the dentin–enamel junction scallop size, the dentin–enamel junction is indeed complex. Their results showed that posterior teeth, which are subject to high masticatory loads, tend to have larger and more pronounced scallops than anterior teeth. It has been suggested that this gradient-like interface improves mechanical performance (32).

The results obtained for maximal loading in the compression test showed that the flat interface design had

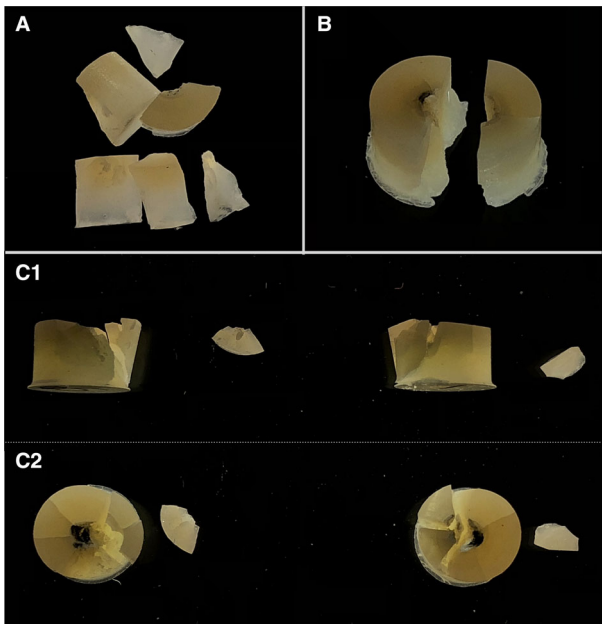

Fig. 4. Photographs of example fracture types: (A) catastrophic bulk fracture; (B) complete bulk failure; (C.1) partial bulk fracture – side view; and (C.2) partial bulk fracture – top view.

the highest load-bearing capacity of all interface designs tested. A potential explanation is that a flat design avoids the introduction of any voids that may act as areas of stress concentration (34, 44). Hence, an interface with a large surface area and a gradient-like design could ultimately present weak points in bilayered structures and cause fracture at lower loads. This phenomenon can be observed in the results reported in this study. We found that designs with a large surface area, such as mesh and pyramid, demonstrated a more extensive and gradient-like design interface. These designs also showed the lowest relative maximum load values in the compression tests. However, it is noteworthy that the maximal unilateral occlusal force reported for posterior composites during function is between 500 and 800 N (45). This is well below the lowest compression loads acquired with any of the designs in this study (1,800 $\pm$ 270 N). Therefore, the maximum compression load applied in all interface designs investigated can be considered as clinically appropriate because they are able to withstand the occasional high occlusal forces experienced during occlusal function (46).

The maximum loads in compression that were recorded, in the present study, for flowable bulk-fill (SDR) and fiber-reinforced (everX) composites are in line with those reported in a similar study by Özyürek *et al.* (47), who utilized the same materials to restore endodontically treated teeth. It was observed that even though the fiber-reinforced composite groups did not demonstrate the highest fracture loads, they had fractures that could be more easily restored (47).

In terms of the effect of interface design and fracture behavior, the results obtained could be explained by the fact that the relatively greater surface area in the pyramid and mesh design provided unique crumple zones. These are similar to those present in cars and human skulls (48). Consequently, they dissipate any incoming crack through the gradient-like interface design and into the bulk material at a lower energy, and the fracture front would have lower energy as it goes through the base material (49). For flowable bulk-fill composite, this means a lower incidence of catastrophic shattering, while in fiber-reinforced composite this translates into the fibers being able to deflect crack propagation away from the bulk of the material and to the peripheries, as was shown in this study. The results are also in line with a previous study showing that in pre-planning for failure in restorations it can be useful to have predictable and favorable failures, when using fibers (48). The presence of such energy-absorbing and stress-distributing fibers results in a higher possibility for repair if failure occurs (50). Similarly, owing to the presence of collagen fibers, it has been reported that the structure of the dentin–enamel junction is comparable with that of a fiber-reinforced structure (51, 52). As a consequence of these findings, the first hypothesis, that fracture behavior would not be affected by the different interface designs, was rejected.

With regard to using different bulk-fill materials and their effect on the fracture behavior of bilayered restorations, there was a general difference between the flowable bulk-fill composite and fiber-reinforced composite groups, as shown in the results. The catastrophic and unfavorable fracture behavior observed for flowable bulk-fill composite is in line with previous studies investigating the mechanical behavior of bulk-fill composites and conventional particulate filler composite (53, 54). Their fundamentally similar material properties thus do not offer significant improvement of fracture propagation, such as partial bulk fractures acquired with fiber-reinforced composite groups (55).

Interestingly, fiber-reinforced composite did not present any instance of catastrophic failure, probably because of the positive reinforcement that fibers provide against fracture, as reported in several studies (56, 57). Such improvement in fracture behavior and toughness was observed in a different study by Abouelleil *et al.* (58), in which the fibers within the matrix held separate fracture ends together, despite the fact that fractures had occurred within test samples. Therefore, the second hypothesis, that there would be no significant differences in fracture behavior using different bulk-fill composite materials, was rejected.

Additionally, 3D profiling was performed on the top surface of bulk-fill composites to confirm whether the designs created on the molds by 3D printing were transferable to the composite surface to create the interface design intended (Fig. 5). There was a small variance, of 0.15 mm, between the mold and the impression. A possible cause could be the viscosity of the bulk-fill materials used in this study (4). On the one hand, fiber-reinforced composite is a packable and more viscous material compared to flowable bulk-fill composite; thus, imprinting an interface design could be appropriately fabricated using firmer pressure and a

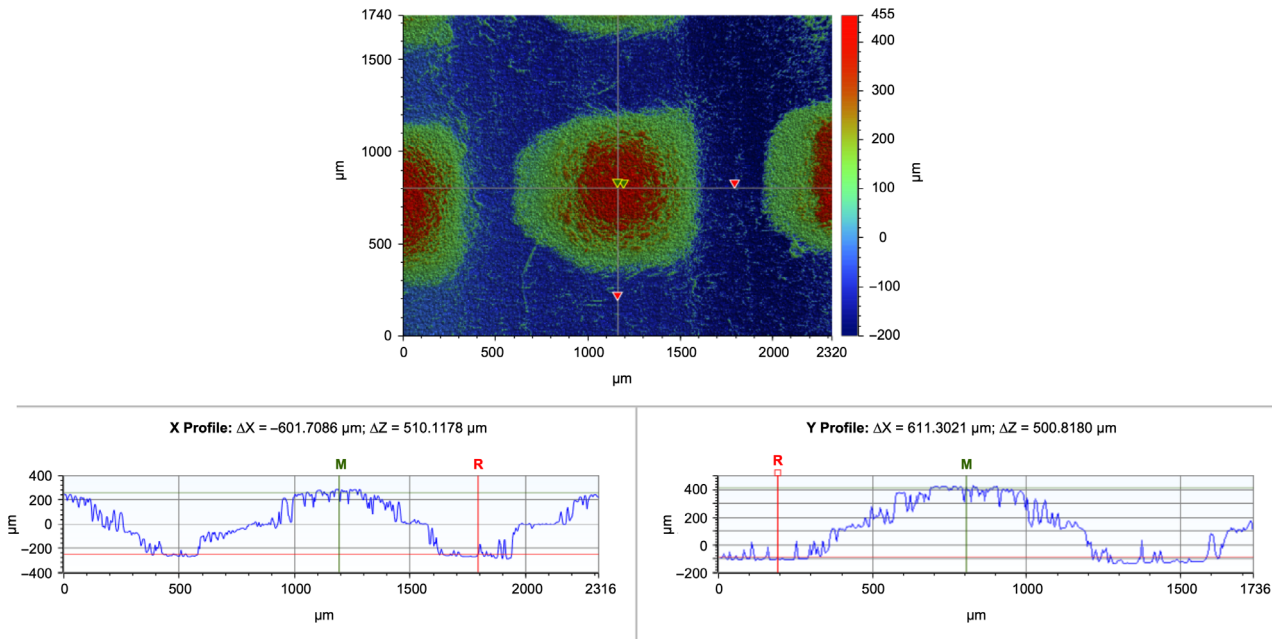

Fig. 5. Three-dimensional (3D) profiling of the mesh interface design. The ΔZ (depth) values were calculated from two reference points (R, M) in the *X* and *Y* profiles.

rigid mold that can apply greater force onto the surface. On the other hand, flowable bulk-fill composite is flowable and less viscous; thus, an interface design can be imprinted easily with the polyvinyl siloxane elastomer mold used in this study.

In this study, a surface microhardness test was performed to evaluate the effect of the light-curing protocol used to create the different interfaces (59). The absence of readings from protocols 1 and 2 infers that interface design imprinting and the light-curing protocol did not have an effect on formation of the oxygen-inhibition layer. This observation can be attributed to the presence of an oxygen-inhibited sticky gel-like layer on the surface of the composite materials, as reported in previous studies (60, 61). This layer of unreacted monomers has a decreased degree of conversion and would thus be soft, and as a result of the softness of the area, the material simply recoils back to normal as the indenter is removed. Therefore, an indent of 245.3 mN was not able to produce any permanent deformations. In a previous study it was shown that protecting the composite surface from ambient oxygen molecules in the air for up to 360 min allowed for higher hardness and effective polymerization (18, 62). This finding is in line with the results for test protocol 3 in which a glass slab was used to cover the surface of the composite for 360 min. Overall, surface microhardness testing is usually most effective when used for metals (61). As a consequence, when applying a load of 245.3 mN, test protocols 1 and 2 showed no measurable indentations in comparison with protocol 3, which was harder and hence indentable.

This study is part of a series of studies aimed at improving the properties of bilayered bulk-fill composite materials. The fabricated interface design in-between two composite materials affected the fracture behavior of bilayered structures. However, this preliminary study only serves as a proof of concept, and further studies are required to be able to make clinical inferences.

A follow-up study on the fracture-toughness properties of each of the interface designs can be a more deductive laboratory parameter for clinical failure, as was demonstrated by Heintze *et al.* (63), in a recent systematic review. In addition, an in-depth analysis of the fracture behavior and stress concentrations along the interface designs could be examined closely by utilizing a technique such as the 3D Finite Element Method (64).

Nonetheless, it is worth mentioning that the tests were conducted through a standardized laboratory protocol, and the clinical situation is variable in terms of handling and placement of material. Furthermore to validate the results of this study clinically, a dynamic load testing procedure should be conducted to quantify the longterm effects of repetitive low occlusal forces on bilayered composite structures.

Within the limitations of this study, the results suggest that the fracture behavior of bilayered composite structures could be affected by the interface design between the base and surface composite layers. Fracture behavior is expected to improve when using short-fiber-reinforced composite as the base material along with an intricate interface design that can improve material failure.

Acknowledgements – This study belongs to the research activity of BioCity Turku Biomaterials and Medical Device Research

Program (www.biomaterials.utu.fi). We would like to deeply thank Dr. Mike Nelson for his help in revising the manuscript.

Conflicts of interest – All authors agreed with the concept of the manuscript and they confirm that there is no economical benefit or any financial interest to report. Authors do not have conflicts of interests. Pekka K. Vallittu declares that he is a consultant for Stick Tech – Member of GC in training and RD.

References

1. Opdam NJM, van de Sande FH, Bronkhorst E, Cenci MS, Bottenberg P, Pallesen U, Gaengler P, Lindberg A, Huysmans MC, van Dijken JW. Longevity of posterior composite restorations: a systematic review and meta-analysis. *J Dent Res* 2014; **93**: 943–949.
2. Ástvaldsdóttir Á, Dagerhamn J, Van Dijken JWV, Naimi-Akbar A, Sandborgh-Englund G, Tranæus S, Nilsson M. Longevity of posterior resin composite restorations in adults – a systematic review. *J Dent* 2015; **43**: 934–954.
3. Schwendicke F, Göstemeyer G, Blunck U, Paris S, Hsu L-Y, Tu Y-K. Directly placed restorative materials: review and network meta-analysis. *J Dent Res* 2016; **95**: 613–622.
4. Pfeifer CS. Polymer-based direct filling materials. *Dent Clin North Am* 2017; **61**: 733–750.
5. Nicola S, Alberto F, Riccardo MT, Allegra C, Massimo SC, Damiano P, Mario A, Elio B. Effects of fiber-glass-reinforced composite restorations on fracture resistance and failure mode of endodontically treated molars. *J Dent* 2016; **53**: 82–87.
6. Heintze SD, Rousson V. Clinical effectiveness of direct class II restorations – a meta-analysis. *J Adhes Dent* 2012; **14**: 407–431.
7. Mount GJ, Tyas MJ, Duke ES, Lasfargues JJ, Kaleka R, Hume WR. A proposal for a new classification of lesions of exposed tooth surfaces. *Int Dent J* 2006; **56**: 82–91.
8. Martins BMC, Silva EJNL, Ferreira DMTP, Reis KR, Fidalgo TKS, Maria de Carvalho Martins B, João Nogueira Leal da Silva E, Masterson Tavares Pereira Ferreira D, Rodrigues Reis K, Kelly da Silva Fidalgo T, de Carvalho Martins BM, Nogueira Leal da Silva EJ, Masterson Tavares Pereira Ferreira D, Rodrigues Reis K, da Silva Fidalgo TK. Longevity of defective direct restorations treated by minimally invasive techniques or complete replacement in permanent teeth: a systematic review. *J Dent* 2018; **78**: 22–30.
9. Lynch CD, Frazier KB, McConnell RJ, Blum IR, Wilson NHF. State-of-the-art techniques in operative dentistry: contemporary teaching of posterior composites in UK and Irish dental schools. *Br Dent J* 2010; **209**: 129–136.
10. Kidd EAM. Clinical threshold for carious tissue removal. *Dent Clin North Am* 2010; **54**: 541–549.
11. Garoushi S, Gargoum A, Vallittu PK, Lassila L. Short fiber-reinforced composite restorations: a review of the current literature. *J Investig Clin Dent* 2018; **9**: e12330.
12. Do T, Church B, Veríssimo C, Hackmyer SP, Tantbirojn D, Simon JF, Versluis A. Cuspal flexure, depth-of-cure, and bond integrity of bulk-fill composites. *Pediatr Dent* 2014; **36**: 468–473.
13. Lassila LVJ, Nagas E, Vallittu PK, Garoushi S. Translucency of flowable bulk-filling composites of various thicknesses. *Chin J Dent Res* 2012; **15**: 31–35.
14. Bucuta S, Ilie N. Light transmittance and micro-mechanical properties of bulk fill vs. conventional resin based composites. *Clin Oral Investig* 2014; **18**: 1991–2000.
15. Omran TA, Garoushi S, Abdulmajeed AA, Lassila LV, Vallittu PK. Influence of increment thickness on dentin bond strength and light transmission of composite base materials. *Clin Oral Investig* 2017; **21**: 1717–1724.
16. Van Ende A, De Munck J, Lise DP, Van Meerbeek B. Bulk-fill composites: a review of the current literature. *J Adhes Dent* 2017; **19**: 95–110.
17. Eliades GC, Caputo AA. The strength of layering technique in visible light-cured composites. *J Prosthet Dent* 1989; **61**: 31–38.
18. Bijelic-Donova J, Garoushi S, Lassila LVJ, Vallittu PK. Oxygen inhibition layer of composite resins: effects of layer thickness and surface layer treatment on the interlayer bond strength. *Eur J Oral Sci* 2015; **123**: 53–60.
19. Chuang SF, Liu JK, Chao CC, Liao FP, Chen YH. Effects of flowable composite lining and operator experience on microleakage and internal voids in class II composite restorations. *J Prosthet Dent* 2001; **85**: 177–183.
20. Leprince JG, Palin WM, Vanacker J, Sabbagh J, Devaux J, Leloup G. Physico-mechanical characteristics of commercially available bulk-fill composites. *J Dent* 2014; **42**: 993–1000.
21. Rosatto CMP, Bicalho AA, Veríssimo C, Bragança GF, Rodrigues MP, Tantbirojn D, Versluis A, Soares CJ. Mechanical properties, shrinkage stress, cuspal strain and fracture resistance of molars restored with bulk-fill composites and incremental filling technique. *J Dent* 2015; **43**: 1519–1528.
22. Yap AUJ, Pandya M, Toh WS. Depth of cure of contemporary bulk-fill resin-based composites. *Dent Mater J* 2016; **35**: 503–510.
23. Abdelmegid F, Salama F, Albogami N, Albabtain M, Alqahtani A. Shear bond strength of different dentin substitute restorative materials to dentin of primary teeth. *Dent Mater J* 2016; **35**: 782–787.
24. Fonseca RB, de Almeida LN, Mendes GAM, Kasuya AVB, Favarão IN, de Paula MS. Effect of short glass fiber/filler particle proportion on flexural and diametral tensile strength of a novel fiber-reinforced composite. *J Prosthodont Res* 2016; **60**: 47–53.
25. Tsujimoto A, Nagura Y, Barkmeier WW, Watanabe H, Johnson WW, Takamizawa T, Latta MA, Miyazaki M. Simulated cuspal deflection and flexural properties of high viscosity bulk-fill and conventional resin composites. *J Mech Behav Biomed Mater* 2018; **87**: 111–118.
26. Garoushi S, Sailynoja E, Vallittu PK, Lassila L. Physical properties and depth of cure of a new short fiber reinforced composite. *Dent Mater* 2013; **29**: 835–841.
27. Bijelic-Donova J, Garoushi S, Lassila LVJ, Keulemans F, Vallittu PK. Mechanical and structural characterization of discontinuous fiber-reinforced dental resin composite. *J Dent* 2016; **52**: 70–78.
28. Garoushi S, Vallittu PK, Lassila L. Mechanical properties and wear of five commercial fibre-reinforced filling materials. *Chin J Dent Res* 2017; **20**: 137–143.
29. Garoushi S, Mangoush E, Vallittu M, Lassila L. Short fiber reinforced composite: a new alternative for direct onlay restorations. *Open Dent J* 2013; **7**: 181–185.
30. Chan YL, Ngan AHW, King NM. Nano-scale structure and mechanical properties of the human dentine–enamel junction. *J Mech Behav Biomed Mater* 2011; **4**: 785–795.
31. White SN, Miklus VG, Chang PP, Caputo AA, Fong H, Sarikaya M, Luo W, Paine ML, Snead ML. Controlled failure mechanisms toughen the dentino-enamel junction zone. *J Prosthet Dent* 2005; **94**: 330–335.
32. Brauer DS, Marshall GW, Marshall SJ. Variations in human DEJ scallop size with tooth type. *J Dent* 2010; **38**: 597–601.
33. Zaytsev D, Panfilov P. Deformation behavior of human enamel and dentin-enamel junction under compression. *Mater Sci Eng C Mater Biol Appl* 2014; **34**: 15–21.
34. Petersen R. Advancing discontinuous fiber-reinforced composites above critical length for replacing current dental composites and amalgam. *J Nat Sci* 2017; **3**: e321.
35. Vallittu P, Özcan M. *A clinical guide to principles of fibre reinforced composites (FRCs) in dentistry*, 1st edn. Cambridge: Woodhead Publishing, 2017; 131–163.
36. Tanner J, Tolvanen M, Garoushi S, Säilynoja E. Clinical evaluation of fiber-reinforced composite restorations in posterior teeth-results of 2.5 year follow-up. *Open Dent J* 2018; **12**: 476–485.

37. Ferracane JL. Correlation between hardness and degree of conversion during the setting reaction of unfilled dental restorative resins. *Dent Mater* 1985; **1**: 11–14.
38. Le Bell AM, Tanner J, Lassila LV, Kangasniemi I, Vallittu PK. Depth of light-initiated polymerization of glass fiber-reinforced composite in a simulated root canal. *Int J Prosthodont* 2003; **16**: 403–408.
39. Yin X, Zhang J, Wang X. Sequential injection analysis system for the determination of arsenic by hydride generation atomic absorption spectrometry. *Fenxi Huaxue* 2004; **32**: 1365–1367.
40. Gayle AJ, Cook RF. Mapping viscoelastic and plastic properties of polymers and polymer-nanotube composites using instrumented indentation. *J Mater Res* 2016; **31**: 2347–2360.
41. Ten Cate AR. *Oral histology: development, structure and function*, 5th edn. St. Louis, MO: Mosby, 1998.
42. Sui T, Lunt AJG, Baimpas N, Sandholzer MA, Li T, Zeng K, Landini G, Korsunsky AM. Understanding nature's residual strain engineering at the human dentine-enamel junction interface. *Acta Biomater* 2016; **32**: 256–263.
43. Smith TM, Olejniczak AJ, Reid DJ, Ferrell RJ, Hublin JJ. Modern human molar enamel thickness and enamel-dentine junction shape. *Arch Oral Biol* 2006; **51**: 974–995.
44. Scotti N, Alovisi C, Comba A, Ventura G, Pasqualini D, Grignolo F, Berutti E. Evaluation of composite adaptation to pulpal chamber floor using optical coherence tomography. *J Endod* 2016; **42**: 160–163.
45. Ledogar JA, Dechow PC, Wang Q, Gharpure PH, Gordon AD, Baab KL, Smith AL, Weber GW, Grosse IR, Ross CF, Richmond BG, Wright BW, Byron C, Wroe S, Strait DS. Human feeding biomechanics: performance, variation, and functional constraints. *PeerJ* 2016; **4**: e2242.
46. Röhrle O, Saini H, Ackland DC. Occlusal loading during biting from an experimental and simulation point of view. *Dent Mater* 2018; **34**: 58–68.
47. Özyürek T, Ülker Ö, Demiryürek EÖ, Yilmaz F. The effects of endodontic access cavity preparation design on the fracture strength of endodontically treated teeth: traditional versus conservative preparation. *J Endod* 2018; **44**: 800–805.
48. Malterud M. Planning for failure: creating dental crumple zones. *Gen Dent* 2014; **62**: 10–13.
49. Rocca GT, Saratti CM, Cattani-Lorente M, Feilzer AJ, Scherrer S, Krejci I. The effect of a fiber reinforced cavity configuration on load bearing capacity and failure mode of endodontically treated molars restored with CAD/CAM resin composite overlay restorations. *J Dent* 2015; **43**: 1106–1115.
50. Karbhari VM, Strassler H. Effect of fiber architecture on flexural characteristics and fracture of fiber-reinforced dental composites. *Dent Mater* 2007; **23**: 960–968.
51. Dong XD, Ruse ND. Fatigue crack propagation path across the dentinoenamel junction complex in human teeth. *J Biomed Mater Res A* 2003; **66**: 103–109.
52. Lin CP, Douglas WH, Erlandsen SL. Scanning electron microscopy of type I collagen at the dentin-enamel junction of human teeth. *J Histochem Cytochem* 1993; **41**: 381–388.
53. Ilie N, Bucuta S, Draenert M. Bulk-fill resin-based composites: an in vitro assessment of their mechanical performance. *Oper Dent* 2013; **38**: 618–625.
54. de Assis FS, Lima SNL, Tonetto MR, Bhandi SH, Pinto SCS, Malaquias P, Loguercio AD, Bandéca MC. Evaluation of bond strength, marginal integrity, and fracture strength of bulk- vs incrementally-filled restorations. *J Adhes Dent* 2016; **18**: 317–323.
55. Isufi A, Plotino G, Grande NM, Ioppolo P, Testarelli L, Bedini R, Al-Sudani D, Gambarini G. Fracture resistance of endodontically treated teeth restored with a bulkfill flowable material and a resin composite. *Ann Stomatol (Roma)* 2016; **7**: 4–10.
56. Ozsevik AS, Yildirim C, Aydin U, Culha E, Surmelioglu D. Effect of fibre-reinforced composite on the fracture resistance of endodontically treated teeth. *Aust Endod J* 2016; **42**: 82–87.
57. Bijelic-Donova J, Uctasli S, Vallittu P, Lassila L. Original and repair bulk fracture resistance of particle filler and short fiber-reinforced composites. *Oper Dent* 2018; **43**: E232–E242.
58. Abouelleil H, Pradelle N, Villat C, Attik N, Colon P, Grosgogeat B. Comparison of mechanical properties of a new fiber reinforced composite and bulk filling composites. *Restor Dent Endod* 2015; **40**: 262–270.
59. Miletic V, Pongprueksa P, De Munck J, Brooks NR, Van Meerbeek B. Curing characteristics of flowable and sculptable bulk-fill composites. *Clin Oral Investig* 2017; **21**: 1201–1212.
60. Vallittu PK. Unpolymerized surface layer of autopolymerizing polymethyl methacrylate resin. *J Oral Rehabil* 1999; **26**: 208–212.
61. Gauthier MA, Stangel I, Ellis TH, Zhu XX. Oxygen inhibition in dental resins. *J Dent Res* 2005; **84**: 725–729.
62. Aromaa MK, Vallittu PK. Delayed post-curing stage and oxygen inhibition of free-radical polymerization of dimethacr ylate resin. *Dent Mater* 2018; **34**: 1247–1252.
63. Heintze SD, Ilie N, Hickel R, Reis A, Loguercio A, Rousson V. Laboratory mechanical parameters of composite resins and their relation to fractures and wear in clinical trials—a systematic review. *Dent Mater* 2016; **33**: e101–e114.
64. Dejak B, Młotkowski A. A comparison of stresses in molar teeth restored with inlays and direct restorations, including polymerization shrinkage of composite resin and tooth loading during mastication. *Dent Mater* 2015; **31**: e77–e87.